Halogen Bonding in Brominated BODIPY Crystals: a Crystallographic and Computational Study

Mónica Farfán-paredes, Pablo Labra-vázquez, Oscar González-antonio, Diego Martínez-bourget, Cristian Guzmán-cedillo, Aylin Galindo-hernández, Margarita Romero, Rosa Santillan, Norberto Farfán

Chemistry–A European Journal
Research Article
doi.org/10.1002/chem.202302847
Chemistry Europe
European Chemical Societies Publishing
www.chemeurj.org

Halogen Bonding in Brominated BODIPY Crystals: a Crystallographic and Computational Study

Mónica Farfán-Paredes,[a] Pablo Labra-Vázquez,[b] Oscar González-Antonio,[c] Diego Martínez-Bourget,[c] Cristian Guzmán-Cedillo,[c] Aylin Galindo-Hernández,[c] Margarita Romero,[c] Rosa Santillan,[a] and Norberto Farfán*[c]

The study of halogen bonds (XBs) has been a subject of great interest in recent years due to its clear application in catalysis, liquid crystals, and crystal engineering. In this study, we analyzed the intermolecular interactions, in particular halogen bonds in BODIPYs with an increasing number of bromine atoms. The computational study included analyses through three different methods: the first approach of close contacts provided by mercury, then the expanded approach of the electron density partition of the molecules in the crystals provided by the analysis of Hirshfeld surfaces, and finally, the approach of the Quantum Theory of Atoms in Molecules (QTAIM) to characterize the non-covalent interactions through finding electron density critical points between atoms and between neighboring molecules. The use of different computational methods allowed to gain insight into the interactions directing the crystal packing as the number of bromine atoms increased in the BODIPY moiety. Monocoordinated and bifurcated halogen bonds involving halide/halide were found. The penta-brominated BODIPY showed four-center cyclic nodes where each node is linked via XBs. This kind of motif can be useful in supramolecular chemistry and self-assembly.

Introduction

A Halogen bond (XB) is a directional noncovalent interaction between an electropositive region of a covalently bound halogen atom (R–X, where X = Cl, Br, or I) and neutral or anionic Lewis bases (B).[1] The electropositive region of a covalently bound halogen arises from the fact that the electrostatic potential around the halogen is anisotropic, this region is known as σ-hole and is oriented 180° to the R–X bond axis. The strong directional preferences of a halogen bond arise from minimizing the exchange repulsion and maximizing the electrostatic and charge transfer attractive contributions to the interaction energy. The strength of the halogen bonds typically decreases in the order I > Br > Cl > F.[1a] A special case of halogen bond arises between two halogens interacting through the positive σ-hole of one halogen and the negative equatorial region of another halogen.[2] There are two types of halogen bonding, Type I and Type II (Figure 1).

Most cases involving XB interactions include two-center contacts (D–A). Whereas bifurcation on the XB acceptor atom is common, the formation of halogen bonds involving bifurcated donors is more unusual.[3] Halogen bonds can also involve π-systems as acceptors and the formation of such halogen bonds is relevant in biological systems.[4] There are bifurcated three-center interactions involving halide/halide and, more recently but more unusual, four-center cyclic nodes where each node is linked via XBs (Figure 2). Isocyanide *trans*-[$PdBr_2(CNC_6H_4$-4-X′$)_2$] (X′ = Br, I) and nitrile *trans*-[$PtX_2(NCC_6H_4$-4-X′$)_2$] (X/X′ = Cl/Cl, Cl/Br, Br/Cl, Br/Br) complexes were reported to form four-center nodes, whereby each node is built up from four Type II C–X′···X–M halogen bond contacts and include one Type I M–X···X–M interaction that form the rhombic-like structure.[5] The structure-directing nodes act as

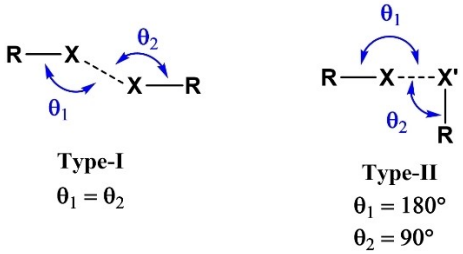

Figure 1. Types of halogen bonding.

[a] Dr. M. Farfán-Paredes, Prof. R. Santillan
Departamento de Química
Centro de Investigación y de Estudios Avanzados del IPN
Av. Instituto Politécnico Nacional 2508, Col. San Pedro Zacatenco, Gustavo A. Madero, C.P. 07360, Ciudad de México (México)

[b] Dr. P. Labra-Vázquez
CIRIMAT, Université de Toulouse
CNRS, Université Toulouse 3–Paul Sabatier
118 Route de Narbonne, 31062 Toulouse Cedex 9 (France)

[c] Dr. O. González-Antonio, D. Martínez-Bourget, C. Guzmán-Cedillo, A. Galindo-Hernández, M. Romero, Prof. N. Farfán
Departamento de Química Orgánica, Facultad de Química
Universidad Nacional Autónoma de México
Av. Universidad 3000, Coyoacán, C.P. 04510, Ciudad de México (México)
E-mail: norberto.farfan@quimica.unam.mx
norberto.farfan@gmail.com

Supporting information for this article is available on the WWW under https://doi.org/10.1002/chem.202302847

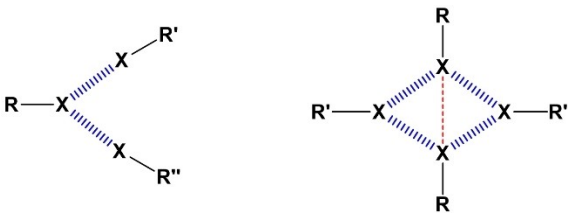

Figure 2. XB interactions involving halide/halide contact.

supramolecular synthons linking metal complexes to form a 2D layered architecture.

Boradiaza-*s*-indacene (BODIPY) chromophores have earned an important place in material science because of their very favorable physicochemical features, including high extinction coefficients and a good absorption at the visible region.[6] Halogenated BODIPYs, besides being excellent building blocks, can serve as effective organic based triplet photosensitizers for a wide range of applications, including photodynamic therapy[7] and photocatalysis.[8] There are a wide variety of halogenated BODIPYs in the literature but the study of halogen bonds in the crystal packing is not always the subject of interest. An interesting study showed that halogen bonding facilitates the formation of the triplet state by increasing the intersystem crossing rate constant of diiodo-BODIPY.[9] Halogen bond is known to play an important role in materials design and crystal engineering, supramolecular chemistry and self-assembly.[3,10] In this study we are interested in analyzing the intermolecular interactions, in particular halogen bonds, in brominated BODIPYs to understand more about the unique nature of halogen bonds and to have new opportunities to use it in the assembly of a wide range of materials.

Results and Discussion

Synthesis of Brominated BODIPYs

Brominated BODIPYs were synthesized starting from 5-bromo-2-thiophenecarboxaldehyde. BODIPY **1** was also synthesized for comparison purposes as previously described.[11] The reaction between 2-thiophenecarboxaldehydes and pyrrole with a catalytic amount of trifluoroacetic acid (TFA) give rise the dipyrromethane precursors **1a** and **2a**. Oxidation with DDQ followed by coordination with $BF_3{\cdot}Et_2O$ gives rise to BODIPYs **1**–**2**.[7a] In order to obtain brominated BODIPY **3**, dipyrromethane **2a** was treated with NBS at −78 °C prior to oxidation and BF_2 complexation (Scheme 1). Brominated BODIPYs **4** and **5** were prepared using molecular Br_2. BODIPY compounds were identified by ^1H, ^{13}C, ^{11}B and ^{19}F nuclear magnetic resonance (NMR) spectroscopy, high resolution mass spectroscopy (HRMS) and for **2**–**4** also by single crystal X-ray diffraction (SXRD).

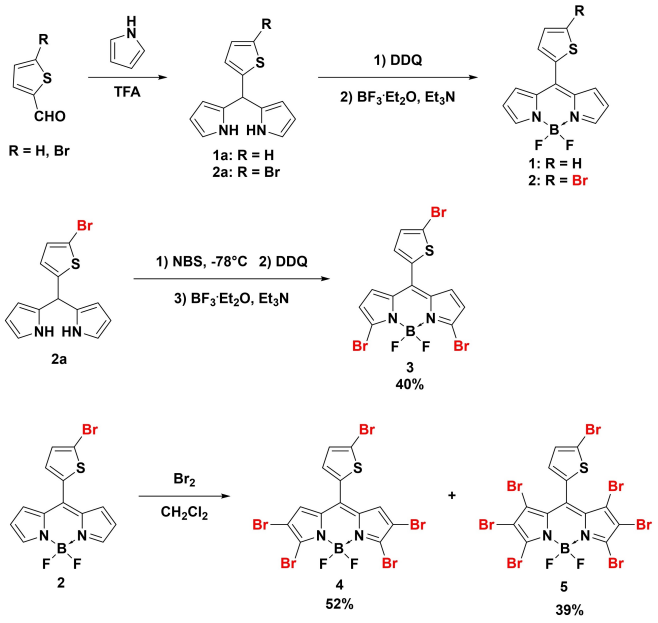

Scheme 1. Synthetic procedure for BODIPYs **1**–**5**.

X-ray Diffraction Analysis

Single crystals of **2**, **3** and **4** were obtained by slow evaporation from hexane/DCM or hexane/acetone solutions. Oak Ridge Thermal Ellipsoid Plot (ORTEP) for BODIPYs **2**–**4** are shown in Figure 3. The molecular structure of BODIPY **2** was solved in the triclinic space group *P*-1 with dihedral angle between thiophene moiety and BODIPY core of 44.69°. The principal interactions were hydrogen bonds and there was a B–F···π interaction (d(B–F2···C5) 3.031 Å, ∠(B–F2···C5) 143.96°) that stacks the BODIPY units face to face in an antiparallel way (Figure 4). The hydrogen bonds found for BODIPYs **2**–**4** are listed in Table 1, hydrogen bonds from BODIPY **1**[12] were also taken for comparative purposes.

BODIPY **3** was solved in the monoclinic space group $P2_1/c$ with dihedral angle of 45.5°. In this case a Br···F halogen bond (*d*(Br···F) 2.878 Å, ∠(C–Br···F) 166.71°) maintains the packing along crystallographic *c* axis (Figure 5), and π···π interaction (*d*(ring A···ring A) 3.477 Å) between pyrrolic rings maintain the BODIPY units in a zigzag arrangement (Figure 6). Additionally, a Br···π interaction was found between the alpha Br3 and pyrrolic ring

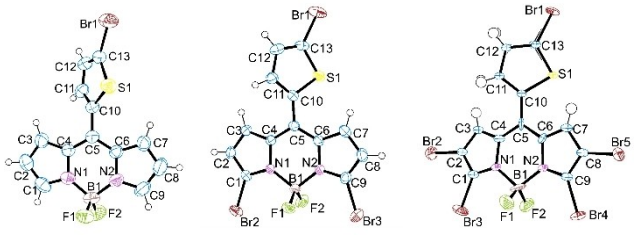

Figure 3. X-ray structures of BODIPYs **2**–**4** from left to right with 50% of ellipsoid probability.

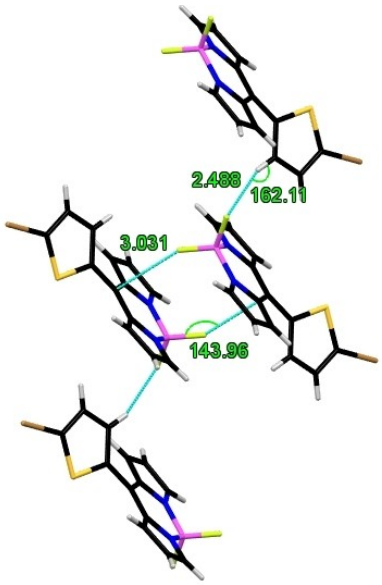

Figure 4. Crystal packing of BODIPY **2** and B–F2···π (*d*(F2···C5) 3.031 Å, ∠(B–F2···C5) 143.96°) and C11-H11···F1 (*d*(H11···F1) 2.488 Å, ∠(C11-H11···F1) 162.11°) interactions.

Table 1. Intermolecular D–H···A interaction parameters (Å and °) for BODIPY compounds.

D–H···A	d(H···A)	d(D–H···A)	D–H···A
BODIPY **1**[17]			
C13–H13···F2	2.485	3.288	144.52°
C11–H11···F2	2.391	3.310	169.56°
C3–H3···F1	2.474	3.282	135.40°
C8–H8···π1	2.770	3.498	133.62°
C3–H3···B	3.108	3.603	111.01°
C11A–H11A···F2	2.561	3.441	158.22°
C13A–H13A···F1	2.600	3.274	129.83°
BODIPY **2**			
C11–H11···F1	2.488	3.385	162.11°
C9–H9···B	3.196	4.105	166.28°
C9–H9···F1	2.553	3.469	168.58°
BODIPY **3**			
C2–H2···F2	2.639	3.197	119.20°
C3–H3···π2	2.793	3.621	148.70°
C7–H7···S	2.836	3.276	110.70°
BODIPY **4**			
C12–H12···F2	2.582	3.173	121.85°

(N1 C1 C2 C3 C4) with 3.586 Å and ∠(C9–Br3···π centroid) 120.65° (Figure 7).

The molecular structure of BODIPY **4** was solved in the triclinic space group *P*-1 with dihedral angle of 40.47°. In this penta-brominated BODIPY most of the interactions found were halogen bonds and all bromine atoms in the molecule interacts between them (Table 2). Before analyzing the halogen bonds in the brominated BODIPYs, a search in the Cambridge Structural

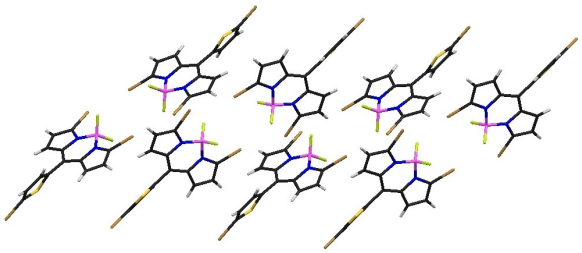

Figure 5. Crystal packing of BODIPY **3** viewed along crystallographic c axis.

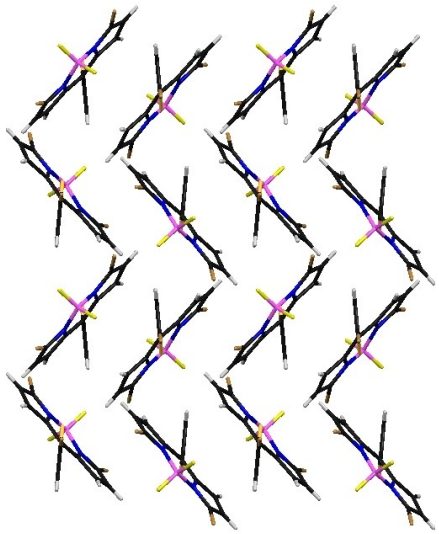

Figure 6. Crystal packing of BODIPY **3** showing a zigzag arrangement.

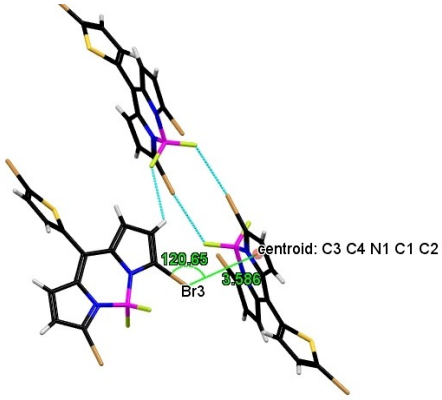

Figure 7. Br···π interaction (*d*(C9Br3···π centroid) 3.586 Å, ∠(C9-Br3···π centroid) 120.65°) in BODIPY **3**.

Table 2. Halogen bond interactions in BODIPY **4**.

R–X···A	d(X···A)	R–X···A (°)
C13Br1···Br2	3.676	143.63
C1Br3···Br5	3.355	172.19
C2Br2···Br1	3.589	158.3
C8Br5···Br5	3.489	132
C9Br4···F1	3.292	162.01

Database (CSD) was carried out and it was found that the maximum Br···Br distance was found to be 3.7 Å and the average distance is 3.572 Å. The (thiophene)Br···Br(β-pyrrolic) interaction accommodates the thiophene units face to face leaving the BODIPY units on opposite sites. The bromine atoms at α-positions (Br3 and Br4) form monocoordinated XBs. Interestingly, the bromine atom at the thiophene and the β-bromine atoms of the BODIPY form a Br···Br···Br···Br parallelepiped between four molecules (Figure 8). The Cambridge Structural Database (CSD) search enabled the recognition of 891 structures with bifurcated halogen bonds in bromine, only 58 form a parallelepiped between bromine atoms. To our knowledge, this constitutes the first report with this motif in an organic molecule since most of the structures that forms this four-center cyclic XB are salts or metal complexes.

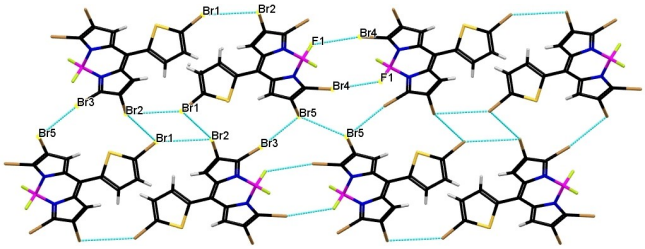

Figure 8. Crystal packing of BODIPY **4** by C13-Br1···Br2 (*d*(Br1···Br2) 3.676 Å, ∠(C13–Br1···Br2) 143.63°), C1–Br3···Br5 (*d*(Br3···Br5) 3.355 Å, ∠(C1–Br3···Br5) 172.19°), C2–Br2···Br1 (*d*(Br2···Br1) 3.589 Å, ∠(C2–Br2···Br1) 158.30°), C8–Br5···Br5 (*d*(Br5···Br5) 3.489 Å, ∠(C8–Br5···Br5) 132.00°) and C9–Br4···F1 (*d*-(Br4···F1) 3.292 Å, ∠(C9–Br4···F1) 162.01°) interactions viewed along *b* axis.

Despite numerous attempts, we were unable to grow crystals of suitable size from BODIPY **5** for single crystal X-ray diffraction. X-ray powder diffraction (PXRD) analysis was carried out and evidence that sample **5** is partly crystalline and partly amorphous (Figure S10). The crystallographic parameters from BODIPYs **2**–**4** are listed in Table 3.

Hirshfeld surface analysis and fingerprint plots

Hirshfeld surface analysis allows a quantitative assessment of the occurrence of supramolecular contacts within a crystal by defining an enveloping surface around a molecule and mapping this surface to obtain information on the closeness of neighboring atoms in relation to those enclosed by the surface.[13] Built

Table 3. Crystallographic data

Identification code	BODIPY **2** CCDC 2291704	BODIPY **3** CCDC 2291705	BODIPY **4** CCDC 2291706
Empirical formula	$C_{13}H_8BF_2N_2SBr$	$C_{13}H_6BF_2N_2SBr_3$	$C_{13}H_4BF_2N_2SBr_5$
Formula weight	352.99	510.8	669.03
Temperature/K	293.15	289(2)	293(2)
Crystal system	triclinic	monoclinic	triclinic
Space group	*P*-1	$P2_1/c$	*P*-1
a, b, c/Å	7.5969(3) 7.9365(3) 11.5458(5)	9.156(3) 12.422(4) 14.233(4)	9.4268(7) 10.1945(7) 10.5818(6)
α, β, γ/°	84.438(2), 85.036(2), 77.127(3)	90, 107.757(9), 90	107.780(6), 101.845(6), 109.842(7)
Volume/Å^3	673.92(5)	1541.7(8)	854.98(11)
Z	2	4	2
ρ_{calcd}g/cm^3	1.74	2.201	2.597
μ/mm^{-1}	3.216	8	15.562
F(000)	348	968	620
Crystal size/mm^3	0.450×0.390×0.270	0.45×0.39×0.27	0.45×0.39×0.27
Radiation	MoKα (λ = 0.71073)	MoKα (λ = 0.71073)	CuKα (λ = 1.54184)
2Θ range for data collection/°	6.126 to 55.008	4.448 to 60.37	9.35 to 146.672
Index ranges	$-9 \le h \le 9$, $-10 \le k \le 10$, $-14 \le l \le 13$	$-12 \le h \le 12$, $-17 \le k \le 17$, $-20 \le l \le 20$	$-11 \le h \le 11$, $-9 \le k \le 12$, $-13 \le l \le 11$
Reflections collected	12849	104565	8501
Independent reflections	3073 [R_{int} = 0.0375, R_{sigma} = 0.0261]	4562 [R_{int} = 0.1125, R_{sigma} = 0.0410]	3334 [R_{int} = 0.0481, R_{sigma} = 0.0590]
Data/restraints/parameters	3073/0/181	4562/0/200	3334/151/212
Goodness-of-fit on F^2	1.052	1.02	1.067
Final R indexes [I >= 2σ (I)]	R_1 = 0.0559, wR_2 = 0.1595	R_1 = 0.0364, wR_2 = 0.0760	R_1 = 0.0487, wR_2 = 0.1229
Final R indexes [all data]	R_1 = 0.0691, wR_2 = 0.1719	R_1 = 0.0713, wR_2 = 0.0872	R_1 = 0.0577, wR_2 = 0.1323
Largest diff. peak/hole / e Å^{-3}	1.43/−1.13	0.78/−0.67	1.10/−1.83

upon the Van der Waals radii of the atoms inside and outside the surface, three distances become relevant: d_i and d_e, which are the distances from the surface to the closest atom inside and outside the surface respectively, and d_{norm}, which represents the sum of d_i and d_e after normalization using the van der Waals radii of the atoms involved. Mapping the Hirshfeld surface with d_{norm} allows a visual assessment of the crystallographic environment of the enclosed molecule; [14] white regions highlight the presence of neighboring atoms outside the surface at a distance around the sum of the van der Waals radii of the enclosed and neighboring atoms, whereas red and blue regions are observed below and above this distance, respectively.

A Hirshfeld surface analysis was conducted for BODIPY derivatives **2**–**4** for which SXRD data could be obtained and whose structures differ on the number of bromine atoms on the fluorophore. The Hirshfeld surfaces for **2**–**4** mapped with d_{norm} are shown in Figure 9, along with crystallographic fragments that allows visualizing relevant supramolecular contacts involving halogen atoms; by partitioning the space within a crystal, these surfaces systematically display regions around the halogen atoms with low d_{norm} values, signaling the presence of noncovalent interactions involving these nuclei with a short interatomic distance and thus with potentially large stabilizing energies.

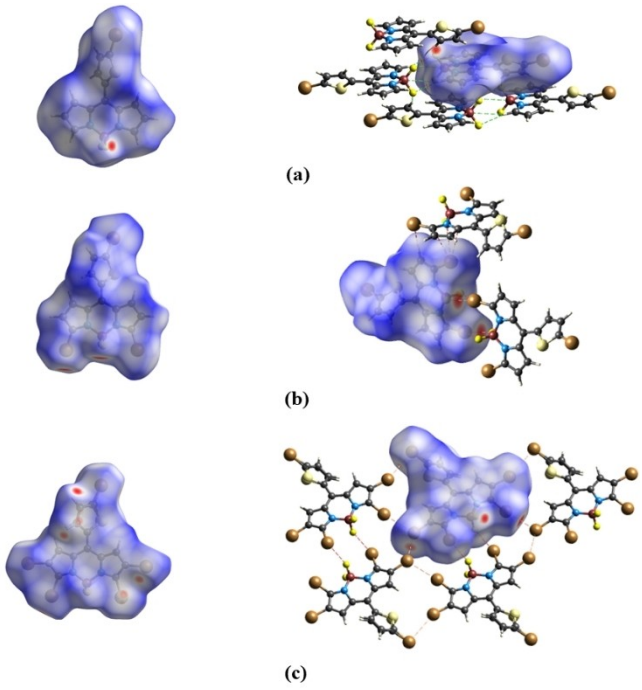

Figure 9. Hirshfeld surfaces (left) and related relevant supramolecular contacts involving halogen atoms (right) for **2** (a), **3** (b) and **4** (c).

These interactions evidently play a more important role in the crystallization of compounds **3** and **4** when compared to **2**, as their variety and occurrence is clearly more important in the former compounds.

To gain quantitative information on the modulation of supramolecular contacts involving halogen atoms in these crystals, we obtained the 2D fingerprint plots for **2**–**4** which are shown in Figure 10 and that provide information on the frequency of supramolecular contacts described by a given pair of d_i and d_e distances, with the frequency being color coded from blue (not frequent) to green and red (frequent). Two general types of contacts involving halogens were inspected: C–H···X and D–X···A, representing potential hydrogen-bonding and halogen-bonding interactions, respectively, and where X = F/Br and A = Br/F/C/N/S. Regarding the C–H···X interactions, a gradual decrease was observed, which can reasonably be attributed to the lower availability of hydrogen atoms within the crystal and to the fact that the most acidic hydrogens within the BODIPY core, and thus the most prone to participate in non-classical HB interactions, are replaced by bromine in **3** and **4** hindering these otherwise favorable interactions.

Perhaps the most important information obtained from this analysis is an apparent correlation between the amount of D–X···A contacts and the number of halogen atoms in the fluorophore, with a major contribution systematically observed for contacts involving the bromine atoms in comparison to B–F···A contacts that displayed a minor contribution remaining relatively unchanged within the series. This trend is remarkably clear for the C–Br···Br contacts whose contributions increases from 0.8% for **2** to 7.9% and 24.2% for **3** and **4**, respectively, accompanied with interatomic distances covering wider ranges for the latter. As shown in Figure 11 these values seem in fact to

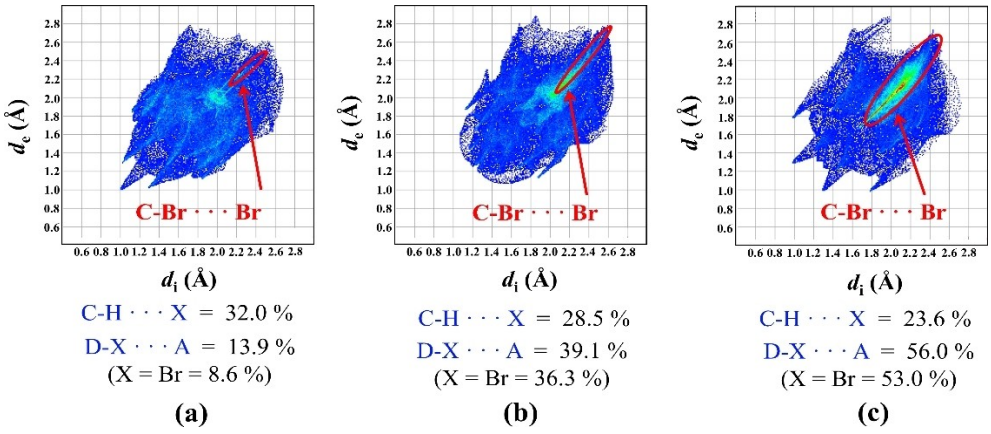

Figure 10. 2D-fingerprint plots and contribution of different supramolecular contacts involving XB (X = F/Br and A = F/Br/C/N/S) for **2** (a), **3** (b) and **4** (c).

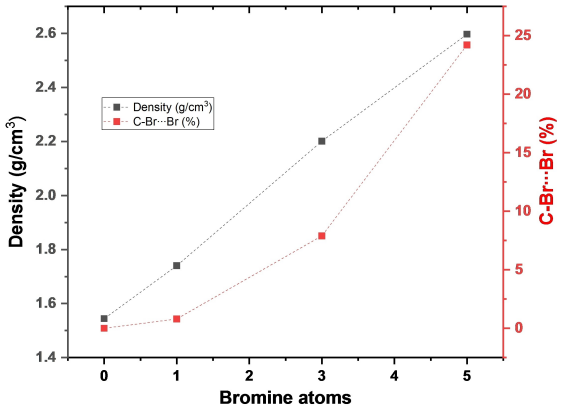

Figure 11. Apparent correlations observed between the number of bromine atoms and the crystal density and the contribution of C–Br···Br contacts to the Hirshfeld surface for compounds **1** (CCDC: 299104)[17] and **2**–**4**.

increase exponentially with the number of bromine atoms leading to a concomitant increase of the crystal density when compared to data extracted from the crystal structure of **1** that was reported elsewhere.[12] Although indicative, these results should nevertheless be taken with care as further examples would be naturally needed to corroborate these apparent dependencies, which if confirmed could lead to interesting crystal engineering applications likely associated to further correlations with optical properties or lattice energies for this type of optical materials.

Analysis through Quantum Theory of Atoms in Molecules

Figure 12 shows the results for the DFT calculations, and the non-covalent interactions calculated through QTAIM methodology as implemented in MultiWFN. Figure 12A depicts the negatively charged fluorine atoms and faint negative strips on the bromine atoms of **3**. The σ-holes for the three bromines were also clearly calculated at the end of these atoms shown in blue and, also in this color, the hydrogen aromatic atoms from pyrrole and thienyl portions are shown. Figure 12B and 12 C contain the visualization of the calculation of the non-covalent interactions. The first is the direct result from the QTAIM approach on the unit cell while the latter is a more schematic representation seen through the lens of chemical intuition.

The fixed portions of **3**, create an electronic environment that favors an intramolecular H-bonding (S–H 2.79 Å, 106.6°) due to the torsion in the *meso*-thienyl group. The most external interactions consist of van der Waals and/or halogen-halogen interactions. Fluorine atoms present two kinds of interactions: H-bonding (2.56–2.61 Å, 115.9°, 171.1°) and halogen-π interactions with neighboring pyrrole portions. Finally, in the central portions of the crystal assembly, π-stacking were also calculated between neighboring pyrrole portions of BODIPYs in the unit cell.

Figure 13 shows the analogous results of this computational study for BODIPY **4**. Figure 13A depicts the ESP map for **4**, which presents a quite similar charge distribution as shown for **3**, with the difference of having two less C–H sites, which are interchanged for two C–Br sites thus changing the nature of these regions from possible CH-π or H-bonding inducers to H-bonding acceptors and halogen interaction inducers. Figures 13B and 13 C contain the visualization of the calculation of the non-covalent interactions. The first is the direct result from the QTAIM approach on the unit cell while the latter is a more schematic representation after applying chemical intuition to it.

A more heavily interacting unit cell can be seen for **4** as obtained with MultiWFN. Also, it is shown that also the fixed rigid portions of **4**, form an intramolecular H-bond (S–H 2.76 Å, 107.7°) and a CH-π contact (2.65 Å) due to the torsion in the *meso*-thienyl group. There are several interactions between the two molecules in the unit cell, like the ones mentioned in the sidenote for Figure 13C, except halogen-π contacts. These latter non-covalent interactions appear only with the neighboring BODIPY in the *c*-axis extension of the unit cell. More H-bonding, van der Waals/halogen-halogen and π-stacking appear in the packing through the c-axis of the unit cell of BODIPY **4** which let

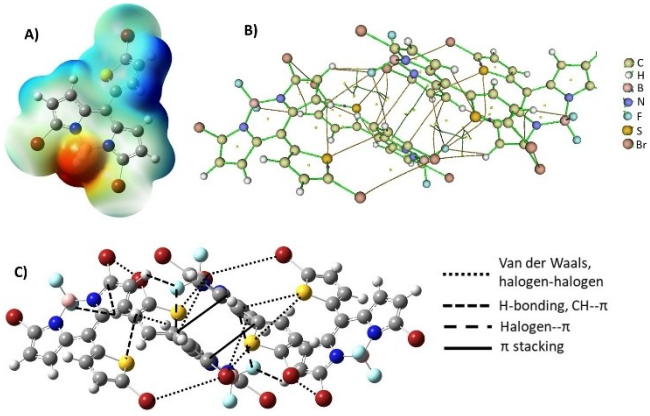

Figure 12. Results of the DFT and the QTAIM computational studies for BODIPY **3**, where A) is the ESP map, B) the MultiWFN visualization of the calculated non-covalent critical points and ring critical points and C) is a schematic representation of the intermolecular contacts directing the crystal packing of **3**.

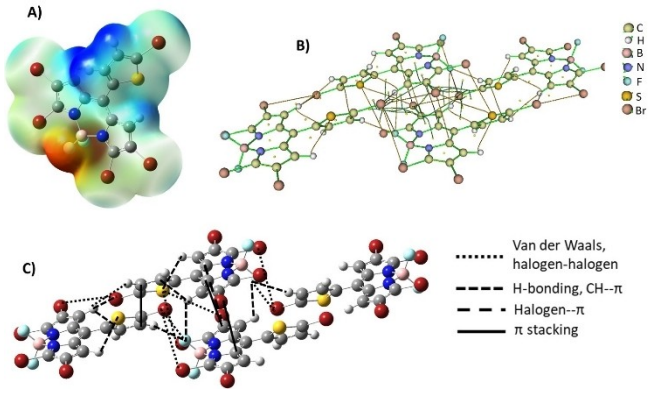

Figure 13. Results of the DFT and the QTAIM computational studies for BODIPY **4**, where A) is the ESP map, B) the MultiWFN visualization of the calculated non-covalent critical points and ring critical points and C) is a schematic representation of the intermolecular contacts directing the crystal packing of **4**.

us gain more insight on how the periodic arrangement is achieved on this axis.

Conclusions

Through different computational methods, a varied series of insights on the intermolecular interactions of BODIPYs with the increased number of bromine atoms were calculated and analyzed. Besides hydrogen bonds in the crystal packing, monocoordinated and bifurcated halogen bonds were found. BODIPY **3** showed a Br···F interaction, which is common in other brominated BODIPYs, as well as a Br···π halogen bond which could be of interest in biological systems. BODIPY **4** showed halogen interactions in each bromine atom. The bromine atoms of the α-positions of the BODIPY core showed monocoordinated halogen bonds, while the bromine atom at thiophene and the bromine atoms at β-positions showed bifurcated halogen bonds that form a four-center parallelepiped. QTAIM results revealed that neighboring cells interact through halogen-halogen/dispersive contacts and between molecules π-stacking and halogen-π were also observed between neighboring pyrroles and bromine atoms. Computational analyses and fingerprint plots showed that there is an increase in Br···Br contacts contributions that depend on the number of bromine atoms.

Experimental Section

General considerations

The starting materials were obtained from commercial sources and used as received. Solvents were distilled over appropriate drying agents. Reactions were monitored by TLC on pre-coated silica gel plates (ALUGRAM SIL G/UV_{254}) and revealed by exposure to a UV_{254} lamp. Infrared spectra (4000–400 cm^{-1}) were recorded on Perkin Elmer 400 FT-IR/FT-FIR. NMR spectra were recorded on Jeol 400 MHz spectrometer and Bruker 500 MHz using deuterated solvents. Chemical shifts data are relative to the residual non deuterated solvent signal, for ^{1}H NMR the reference signal was fixed at $\delta =$ 7.26 ppm and for ^{13}C NMR at $\delta = 77$ ppm for $CDCl_3$ and $\delta = 5.32$ ppm and $\delta = 54$ ppm in CD_2Cl_2 for ^{1}H and ^{13}C NMR respectively.

Single crystal XRD studies

X-ray crystallographic data was obtained with Bruker APEX II diffractometer with a CCD area detector (MoKα = 0.71073 Å, monochromator: graphite, T = 298 K). The heavier atoms were found by Fourier map difference and refined anisotropically. All reflection data set were corrected for polarization effects. Indexing, data integration and reduction were carried out using APEX. The structures were solved using SHELXT[15] and then refined by full matrix least squares refinements on F^2 using the SHELXL.[16] Mercury[17] and ORTEP[18] programs were used to prepare artwork representations. Hirshfeld surfaces and 2D fingerprint plots were generated using CrystalExplorer 17.[19]

Deposition Numbers 2291704 (for **2**), 2291705 (for **3**), 2291706 (for **4**) contain the supplementary crystallographic data for this paper. These data are provided free of charge by the joint Cambridge Crystallographic Data Centre and Fachinformationszentrum Karlsruhe Access Structures service.

Computational Methodology

Single molecule calculations for BODIPYs **3** and **4**, were performed to optimize and obtain the ground state geometry and the cube for the electrostatic potential (ESP) maps shown in Figures 12 and 13. This was done *via* a DFT approach at a M06-2X/def2SVP level of theory, a functional and basis set size that can describe geometries and non-covalent interactions[20] with a good level of accuracy at an accessible computational cost. An SMD solvation model in chloroform was also used for these calculations.

From the coordinates coming from the CIF file of the corresponding crystals the unit cell was corrected for the electron density of the hydrogen atoms, allowing the structure to relax or correct during the optimization only for these atoms, maintaining the position of the other atoms of the unit cells, which is known to be a widespread protocol to approach computational studies on crystals.[21] The same level of theory used for the single molecule optimizations was used for these calculations. For BODIPY **3** the unit cell with Z = 4 was used directly while for BODIPY **4** we deemed the Z = 2 would require more information for a more complete description of the crystal packing, and it was decided to extend the unit cell trough *c* axis to also have 4 molecules to study the non-covalent interactions. All calculations up to this point were carried put using Gaussian 16 software and GaussView 5.0 visualization suite.[22]

From the crystal calculations, a wfn output file was obtained to use as input for a complete non-covalent interaction calculation and characterization using the MultiWFN software[23] via a QTAIM approach.

Synthesis and Characterization

3,5-dibromo-8-(5′-bromothiophen-2′-yl)-4,4-difluoro-4-bora-3a,4a-diaza-*s*-indacene (**3**). 5-bromo-2-thiophenecarboxaldehyde (0.7 mL, 5.5 mmol) and pyrrole (2.0 mL, 27.6 mmol) were mixed and then trifluoroacetic acid was added. The solution was stirred for 15 min at room temperature, at this point no starting aldehyde was shown by TLC analysis. The mixture was diluted with dichloromethane and washed with water. The organic phase was dried with Na_2SO_4, and the solvent was removed under reduced pressure. Dipyrromethane previously prepared was dissolved in 15 mL of anhydrous THF under N_2 atmosphere at −78 °C. In another round-bottom flask, NBS was dissolved in anhydrous THF under same conditions. The NBS solution was added to the dipyrromethane solution and stirred at −78 °C for 1 h. The reaction mixture was allowed to reach room temperature and DDQ was added and stirring was continued for 1 additional hour followed by addition of Et_3N and $BF_3{\cdot}Et_2O$. After stirring for another hour, the reaction mixture was washed with water and dried with Na_2SO_4, and the solvent was evaporated. The product was purified by flash chromatography (silica gel, hexane/acetone 98 : 2) and yielded 33 % of the BODIPY. Mp: 166–167 °C. FTIR-ATR (υ, cm^{-1}): 3638, 3405, 2969, 2930, 1707, 1540, 1374, 1298, 1251, 1075, 967, 944. UV/Vis (λ, nm): 536. ^{1}H NMR [400 MHz, $CDCl_3$] (δ, ppm): 7.25 (d, $J =$ 3.9 Hz, 1H), 7.23 (d, $J = 3.9$ Hz, 1H), 7.13 (d, $J = 3.9$ Hz, 2H), 6.58 (d, $J =$ 4.0 Hz, 2H). ^{13}C NMR [100 MHz, $CDCl_3$] (δ, ppm): 134.7, 134.2, 133.8, 133.0, 132.9, 131.3, 123.0, 122.9, 118.9. ^{11}B NMR [128 MHz, $CDCl_3$] (δ, ppm) : 0.49 (t, $J_{[B\text{-}F]} = 28$ Hz). ^{19}F NMR [282 MHz, $CDCl_3$] (δ, ppm): −146.19 (q, $J_{[B\text{–}F]} = 28$ Hz). HRMS (ESI-TOF) (m/z): 488.7868 [M^+–F], calcd $C_{13}H_6BN_2FSBr_3$: 488.7873.

2,3,5,6-tetrabromo-8-(5′-bromothiophen-2′-yl)-4,4-difluoro-4-bora-3a,4a-diaza-*s*-indacene (**4**). BODIPY **2** (291 mg, 0.8 mmol) was dissolved in CH_2Cl_2 (30 mL) and then molecular Br_2 (6 eq. 5 mmol) previously dissolved in CH_2Cl_2 (20 mL) was added dropwise to the solution. The reaction was stirred along 2 h until total consumption of starting material. The product was purified by flash chromatog-

raphy (silica gel, hexane/acetone 99.5:0.5) and yielded 52% of the BODIPY **4**. Mp: 210–212 °C. FTIR-ATR (υ, cm^{-1}): 2962, 1257, 1080, 1009, 787. UV/Vis (λ, nm): 555. ^{1}H NMR [500 MHz, $CDCl_3$] (δ, ppm): 7.29 (d, J = 4.8 Hz, 1H, H-4′), 7.27 (d, J = 4.8 Hz, 1H, H-3′), 7.24 (s, 2H, H-1,7). ^{13}C NMR [100 MHz, $CDCl_3$] (δ, ppm) 135.5, 134.1, 133.8, 133.7, 133.5, 131.9, 131.2, 120.5, 112.6. ^{11}B NMR [128 MHz, $CDCl_3$] (δ, ppm): −0.81 (t, $J_{[B-F]}$ = 28 Hz). ^{19}F NMR [282 MHz, $CDCl_3$] (δ, ppm): −147.85 (q, $J_{[B-F]}$ = 28 Hz). HRMS (ESI-TOF) (m/z): 644.6085 [M^+–F], calcd $C_{13}H_4BN_2FSBr_5$: 644.6089.

1,2,3,5,6,7-hexabromo-8-(5′-bromothiophen-2′-yl)-4,4-difluoro-4-bora-3a,4a-diaza-*s*-indacene (**5**). Same procedure previously described. The product was purified by flash chromatography (silica gel, hexane/acetone 99.9:0.1) and yielded 39% of BODIPY **5**. Mp: sublimates to 320°. FTIR-ATR (υ, cm^{-1}): 1517, 1350, 1275, 1112. UV/Vis (λ, nm): 570. ^{1}H NMR [500 MHz, CD_2Cl_2] (δ, ppm): 7.21 (d, J = 4 Hz, 1H), 6.91 (d, J = 4 Hz, 1H). ^{13}C NMR [125 MHz, CD_2Cl_2] (δ, ppm): 136.5, 134.5, 132.6, 131.8, 131.9, 130.8, 124.5, 118.6, 117.0. ^{11}B NMR [160 MHz, CD_2Cl_2] (δ, ppm): −0.98 (t, $J_{[B-F]}$ = 28 Hz). ^{19}F NMR [470 MHz, CD_2Cl_2] (δ, ppm): −145.45 (q, $J_{[B-F]}$ = 28 Hz). HRMS (ESI-TOF) (m/z): 819.4279 [M^+], calcd. $C_{13}H_2BN_2F_2SBr_7$: 819.4283.

Supporting Information

NMR Spectra and geometric parameters of the BODIPY compounds are in the Supporting Information.

Acknowledgements

Authors thanks Marco Leyva for XRD acquisition. M.F-P (CVU 580380) and O.G-A (CVU 289250) thank CONAHCYT for their postdoctoral fellowships. N.F. thanks CONAHCYT (AI-S -7642), PAIP, PAPIIT (IN200422). UNAM-DGTIC for the supercomputing resources through Project "LANCAD-UNAM-DGTIC-268"

Conflict of Interests

The authors declare no conflict of interest.

Data Availability Statement

The data that support the findings of this study are openly available in The Cambridge Crystallographic Data Centre at https://www.ccdc.cam.ac.uk, reference number 2291704.

Keywords: BODIPYs · crystal engineering · halogen bonding · sigma holes

[1] a) X. Ding, M. Tuikka, M. Haukka, *Halogen bonding in crystal engineering.* Vol. 262. **2012**: IntechOpen London, UK; b) P. Metrangolo, F. Meyer, T. Pilati, G. Resnati, G. Terraneo, *Angew. Chem. Int. Ed.* **2008**, *47(33)*, 6114–6127.
[2] G. Cavallo, P. Metrangolo, R. Milani, T. Pilati, A. Priimagi, G. Resnati, G. Terraneo, *Chem. Rev.* **2016**, *116(4)*, 2478–2601.
[3] J.-C. Christopherson, F. Topić, C. Barrett, T. Friščić, *Cryst. Growth Des.* **2018**, *18(2)*, 1245–1259.
[4] H. Matter, M. Nazaré, S. Güssregen, D. W. Will, H. Schreuder, A. Bauer, M. Urmann, K. Ritter, M. Wagner, V. Wehner, *Angew. Chem. Int. Ed.* **2009**, *48(16)*, 2911–2916.
[5] M. A. Kryukova, D. M. Ivanov, M. A. Kinzhalov, A. S. Novikov, A. S. Smirnov, N. A. Bokach, V. Yu. Kukushkin, *Chem. Eur. J.* **2019**, *25(60)*, 13671–13675.
[6] a) R. Ziessel, G. Ulrich, A. Harriman, *New J. Chem.* **2007**, *31(4)*, 496–501; b) S. Niu, G. Ulrich, P. Retailleau, R. Ziessel, *Tetrahedron Lett.* **2011**, *52(38)*, 4848–4853.
[7] a) V.-C. Alejandro, F.-P. Mónica, A.-P. Xelha, R. Mario, R.-O. Gabriel, F. Norberto, R.-G. Eva, *Polyhedron* **2020**, *176*, 114207; b) J. H. Gibbs, L. T. Robins, Z. Zhou, P. Bobadova-Parvanova, M. Cottam, G. T. McCandless, F. R. Fronczek, M. G. H. Vicente, *Bioorg. Med. Chem.* **2013**, *21(18)*, 5770–5781.
[8] a) G. Magagnano, A. Gualandi, M. Marchini, L. Mengozzi, P. Ceroni, P. Cozzi, *Chem. Commun.* **2017**, *53(10)*, 1591–1594; b) W. H. García-Santos, J. Ordóñez-Hernández, M. Farfán-Paredes, H. M. Castro-Cruz, N. A. Macías-Ruvalcaba, N. Farfán, A. Cordero-Vargas, *J. Org. Chem.* **2021**, *86(23)*, 16315–16326.
[9] Y. Lee, R. M. Malamakal, D. M. Chenoweth, J. M. Anna, *J. Phys. Chem. Lett.* **2020**, *11(3)*, 877–884.
[10] a) L. C. Gilday, S. W. Robinson, T. A. Barendt, M. J. Langton, B. R. Mullaney, P. D. Beer . *Chem. Rev.* **2015**, *115(15)*, 7118–7195; b) B. K. Saha, A. Nangia, M. Jaskólski, *CrystEngComm.* **2005**, *7(58)*, 355–358.
[11] J. Songkhao, R. Banerjee, S. Debnath, S. Narasimhan, N. Wannaprom, P. Vanalabhpatana, N. Seriani, R. Gebauer, P. Thamyongkit, *Dyes Pigm.* **2017**, *142*, 558–571.
[12] S. H. Choi, K. Kim, J. Lee, Y. Do, D. G. Churchill, *J. Chem. Crystallogr.* **2007**, *37*, 315–331.
[13] M. A. Spackman, D. Jayatilaka, *CrystEngComm* **2009**, *11(1)*, 19–32.
[14] J. J. McKinnon, D. Jayatilaka, M. A. Spackman, *Chem. Commun.* **2007**, *(37)*, 3814–3816.
[15] G. M. Sheldrick, *Acta Crystallogr. A: Found. Adv.* **2015**, *71(1)*, 3–8.
[16] G. M. Sheldrick, *Acta Crystallogr. C: Struct. Chem.* **2015**, *71(1)*, 3–8.
[17] C. F. Macrae, I. Sovago, S. J. Cottrell, P. T. Galek, P. McCabe, E. Pidcock, M. Platings, G. P. Shields, J. S. Stevens, M. Towler, *J. Appl. Crystallogr.* **2020**, *53(1)*, 226–235.
[18] L. J. Farrugia, *J. Appl. Crystallogr.* **2012**, *45(4)*, 849–854.
[19] P. R. Spackman, M. J. Turner, J. J. McKinnon, S. K. Wolff, D. J. Grimwood, D. Jayatilaka, M. A. Spackman, *J. Appl. Crystallogr.* **2021**, *54(3)*, 1006–1011.
[20] a) M. Iker, A. J. A. Harvey, A. Sen, C. E. H. Dessent, *J. Phys. Chem. A* **2013**, *117 (47)*, 12590–12600; b) B. C. Ferrari, C. J. Bennett, *J. Phys. Conf. Ser.* **2019**, *1290*, 012013; c) N. Mardirossian, M. Head-Gordon, *J. Chem. Theory Comput.* **2016**, *12(9)*, 4303–4325.
[21] a) M. G. Siskos, M. I. Choudhary, I. P. Gerothanassis, *Molecules* **2017**, *22*, 415; b) A. L. Reviglio, F. A. Martínez, M. D. A. Montero, Y. G. Linck, G. A. Aucar, N. R. Sperandeo, G. A. Monti, *RSC Adv.* **2021**, *11*, 7644–7652; c) A. Cedillo-Cruz, D. Martínez-Otero, J. Barroso-Flores, E. Cuevas-Yañez, *J. Mol. Struct.* **2022**, *1264*, 133225.
[22] M. J. Frisch, G. W. Trucks, H. B. Schlegel, G. E. Scuseria, M. A. Robb, J. R. Cheeseman, G. Scalmani, V. Barone, G. A. Petersson, H. Nakatsuji, X. Li, M. Caricato, A. V. Marenich, J. Bloino, B. G. Janesko, R. Gomperts, B. Mennucci, H. P. Hratchian, J. V. Ortiz, A. F. Izmaylov, J. L. Sonnenberg, Williams, F. Ding, F. Lipparini, F. Egidi, J. Goings, B. Peng, A. Petrone, T. Henderson, D. Ranasinghe, V. G. Zakrzewski, J. Gao, N. Rega, G. Zheng, W. Liang, M. Hada, M. Ehara, K. Toyota, R. Fukuda, J. Hasegawa, M. Ishida, T. Nakajima, Y. Honda, O. Kitao, H. Nakai, T. Vreven, K. Throssell, J. A. Montgomery Jr., J. E. Peralta, F. Ogliaro, M. J. Bearpark, J. J. Heyd, E. N. Brothers, K. N. Kudin, V. N. Staroverov, T. A. Keith, R. Kobayashi, J. Normand, K. Raghavachari, A. P. Rendell, J. C. Burant, S. S. Iyengar, J. Tomasi, M. Cossi, J. M. Millam, M. Klene, C. Adamo, R. Cammi, J. W. Ochterski, R. L. Martin, K. Morokuma, O. Farkas, J. B. Foresman, D. J. Fox, *Gaussian 16 Rev. C.01*. 2016: Wallingford, CT.
[23] T. Lu, F. Chen, *J. Comput. Chem.* **2012**, *33(5)*, 580–592.

Manuscript received: August 31, 2023
Accepted manuscript online: September 24, 2023
Version of record online: ■■, ■■

RESEARCH ARTICLE

The intermolecular interactions, in particular halogen bonds (XB) in BODIPYs, were analyzed with the increasing number of bromine atoms. Monocoordinated and bifurcated halogen bonds were found, and a rhombic-like structure was formed by XB interactions. Computational analyses and fingerprint plots showed that there is an increase in Br···Br contacts contributions that depend on the number of bromine atoms.

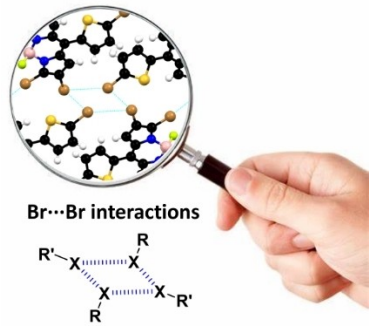

*Dr. M. Farfán-Paredes, Dr. P. Labra-Vázquez, Dr. O. González-Antonio, D. Martínez-Bourget, C. Guzmán-Cedillo, A. Galindo-Hernández, M. Romero, Prof. R. Santillan, Prof. N. Farfán**

1 – 9

Halogen Bonding in Brominated BODIPY Crystals: a Crystallographic and Computational Study